Mol Divers (2015) 19:931–943
DOI 10.1007/s11030-015-9612-4

FULL-LENGTH PAPER

Modelling the molecular mechanism of protein–protein interactions and their inhibition: CypD–p53 case study

S. M. Fayaz[1] · **G. K. Rajanikant**[1]

Received: 5 January 2015 / Accepted: 1 July 2015 / Published online: 14 July 2015

Abstract Cyclophilin D (CypD) is an important regulatory protein involved in mitochondrial membrane permeability transition and cell death. Further, the mitochondrial CypD–p53 axis is an important contributor to necroptosis, a form of programmed necrosis, involved in various cardiovascular and neurological disorders. The CypD ligand, Cyclosporin A (CsA), was identified as an inhibitor of this interaction. In this study, using computational methods, we have attempted to model the CypD–p53 interaction in order to delineate their mode of binding and also to disclose the molecular mechanism, by means of which CsA interferes with this interaction. It was observed that p53 binds at the CsA-binding site of CypD. The knowledge obtained from this modelling was employed to identify novel CypD inhibitors through structure-based methods. Further, the identified compounds were tested by a similar strategy, adopted during the modelling process. This strategy could be applied to study the mechanism of protein–protein interaction (PPI) inhibition and to identify novel PPI inhibitors.

Keywords Cyclophilin D · Cyclosporin A · Necroptosis · Neurological disorders · p53 · Protein–protein interactions

Introduction

Cyclophilin D (CypD), also known as peptidyl prolyl cis-trans isomerase F (PPIF), is a mitochondrial protein that is involved in the necroptosis-mediated cell death [1]. During cell death, CypD residing in the matrix of mitochondria relocates and associates with the inner mitochondrial membrane to form a mitochondrial permeability transition pore (MPTP). It is recognized as a crucial component for MPTP formation [2,3]. Certain physiological stress conditions, such as oxidative stress, drive towards the long-lasting opening of MPTP which leads to the mitochondrial permeability transition (MPT) [4]. MPT is witnessed by an abrupt increase of inner mitochondrial membrane permeability, irreversible loss of mitochondrial membrane potential and production of reactive oxygen species (ROS). All these events will ultimately lead to cell death [5,6].

CypD-mediated necroptotic cell death was reported in various neurological disorders, such as Alzheimer's disease, Parkinson's disease, Huntington disease, cerebral ischemia, traumatic brain injury and spinal cord injury [7–11]. It regulates MPT and controls necroptosis in these diseases [2,12]. Hence, CypD is considered as an attractive pharmacological target in clinical practice [13].

Recent studies have reported that, during oxidative stress, p53 could open the MPTP to trigger necrosis [1]. To achieve this, p53 accumulates and interacts with CypD in the mitochondrial matrix that triggers MPTP opening and necrosis. Formation of the p53–CypD complex was observed in neurological disorders, such as cerebral ischemia/reperfusion (I/R) injury. Further, p53 was localized to the mitochon-

Electronic supplementary material The online version of this article (doi:10.1007/s11030-015-9612-4) contains supplementary material, which is available to authorized users.

✉ G. K. Rajanikant
rajanikant@nitc.ac.in

[1] School of Biotechnology, National Institute of Technology Calicut, Calicut 673601, India

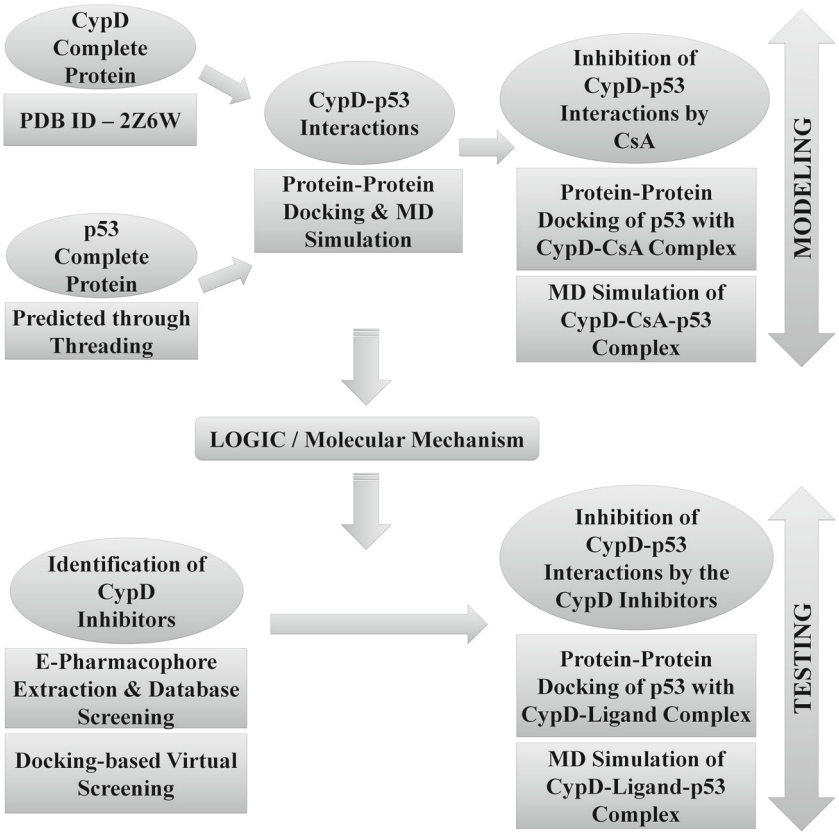

Fig. 1 Study workflow. Elucidation of the molecular mechanism behind the inhibition of CypD–p53 interaction and the identification of potential CypD inhibitors

dria inducing oxidative stress. Thus, it was suggested that, in response to oxidative stress, p53 participates in necroptosis by interacting directly with CypD to open the PTP. In contrast, reduction of p53 levels or pre-treatment with the CypD inhibitor, Cyclosporin A (CsA), prevented this complex formation [1]. Hence, inhibition of the CypD–p53 interaction was suggested to be a better therapeutic strategy in the diseases involving necroptosis. However, the binding mode of CypD with p53, and the molecular mechanism behind the inhibition of CypD–p53 interaction by CsA are not known. Further, CsA is not a drug of choice owing to its limitations, such as poor solubility and bioavailability, bulky nature and cross reactivity [14–19]. Thus, there is a need for the identification of novel small molecule inhibitors of the CypD–p53 interaction to protect cells from necroptotic cell death.

Knowledge regarding the binding mode of CypD–p53 is essential in order to inhibit this interaction. Further, the mechanism by which CsA inhibits CypD–p53 interaction needs to be uncovered. Therefore, in the present study, protein–protein docking followed by molecular dynamics (MD) simulation was carried out to understand the binding modes and the molecular interactions of CypD and p53. Further, CypD–p53 complex was simulated in the presence of CsA to understand the mechanism of inhibition of this interaction by CsA. The knowledge thus derived was employed to identify potential CypD inhibitors (Fig. 1).

Materials and methods

Protein structures

The complete protein 3D (three-dimensional) structures of CypD and p53 are required to identify their binding modes with each other. Since the complete structure of the CypD protein is available in the PDB, the structure with best resolution (PDB ID: 2Z6W) was used for this study.

On the other hand, the complete 3D structure of p53 is not available in the PDB. The 3D structure of p53 could not be identified through homology modelling since it does not contain any 3D protein template with maximum identity and sequence coverage. Hence, its structure was predicted through threading using the I-TASSER server [20]. Iterative Threading ASSEmbly Refinement (I-TASSER) is a computational method for 3D protein structure prediction. Structural templates are detected from the PDB by fold recognition or threading. The full-length structure models are constructed by reassembling structural fragments from threading templates using replica exchange Monte Carlo simulations. Thus, the model with the best C-Score was selected and was further verified through PROCHECK and the Ramachandran plot hosted by the structural analysis and verification server (SAVES) (http://nihserver.mbi.ucla.edu/SAVS/). PROCHECK is a program

to check the stereochemical quality of protein structures by analyzing residue-by-residue geometry and overall structure geometry.

The availability of protein 3D structures is essential for rational drug design. The protein structures determined via experimental methods, such as X-ray crystallography and NMR spectroscopy, are more reliable compared to the structures predicted through *in silico* methods. However, experimental methods are time-consuming and expensive. Further, not all proteins can be successfully crystallized (i.e., membrane proteins) [21–26]. Hence, the structural information of a series of protein 3D structures and their interactions were developed in a timely manner, by means of structural bioinformatics techniques [27–33]. Similarly, the computational protein structure prediction technique was adopted in the current study also.

The 3D structures of CypD and p53 proteins were prepared using the protein preparation wizard of Schrodinger (Schrodinger LLC., Portland, USA) as described earlier [34] and were further considered for pharmacophore analysis and docking.

Protein–protein docking

Protein–protein interactions play a key role in cellular processes and pathways. Numerous computational methods, such as protein–protein docking, have been proposed to predict these interactions to provide insight into cell signalling mechanisms [35–39].

To study the CypD–p53 interactions, molecular docking of these proteins was performed through the ZDOCK server v3.0.2 [40]. p53 and CypD were considered as the receptor and the ligand, respectively. The proteins were docked based on IFACE statistical potential, shape complementarity and electrostatics. The protein–protein complex with the best ZDOCK score was considered for molecular dynamics (MD) simulation.

e-Pharmacophore extraction

Fragment-based energy-optimized pharmacophore (e-pharmacophore) was extracted to identify all the energetically favourable pharmacophore features in the CypD-binding site [34]. The Glide fragment library was docked into the binding site of the protein using Glide XP (Glide v5.7, Schrodinger LLC., New York, NY). The resulting pose viewer file was used to generate the pharmacophore through e-pharmacophore script in the Schrodinger software. Pharmacophore sites were automatically generated from the protein–fragments complex through the Phase module of the Schrodinger suite.

Pharmacophore validation

The extracted e-pharmacophore was validated using the CypD inhibitors reported in the PDB (PDB IDs: 3RCF, 3RDC, 4J58, 4J59, 4J5A, 4J5B, 4J5C, 4J5D and 4J5E). These compounds were prepared by the LigPrep module of the Schrodinger suite (LigPrepv2.3, Schrodinger, LLC, New York, NY). The ligands were processed to assign the suitable protonation states at physiological pH 7.2 ± 0.2. Conformer generation was carried out with the ConfGen torsional sampling using the OPLS 2005 force field.

These inhibitors were seeded randomly into the ZINC compound database, and pharmacophore-based screening was carried out. Enrichment factor (EF) was employed to validate the extracted e-pharmacophore. EF is one of the best methods to evaluate the effectiveness of a virtual screening protocol [41,42]. The EF is defined as follows:

$$\mathrm{EF}^{x\%} = \frac{n(\text{active at } x\%)/n(x\%)}{n(\text{all active})/n(\text{all})},$$

where n(active at $x\%$) is the number of active ligands identified in the top $x\%$ of the database screened, $n(x\%)$ is the number of compounds screened at top $x\%$ of the database, n(all active) is the number of active ligands in the entire database and n(all) is the number of compounds in the entire database.

The pharmacophore was validated using the early EFs at 1 and 5 % of the database screened.

Pharmacophore-based screening

The extracted fragment-based e-pharmacophore of CypD was employed to screen the lead-like compounds (~2 million unique structure records) in the ZINC database [43] using the Phase module. For filtering the database molecules, distance matching tolerance was set to 2.0 Å and the matching of a minimum of 4 sites was set as criterium. The ligand conformers that matched well with the hypothesis were obtained as output and were ranked in the order of their fitness score. All the compound hits, thus obtained, were considered for protein–ligand docking.

Protein–ligand docking

The compound hits, obtained through pharmacophore-based screening, were prepared and their conformers were generated as described in the earlier section. Glide energy grid was generated from the CypD protein structure. The co-crystallized ligand was differentiated from the active site of the receptor and the grid was defined by a rectangular box surrounding the ligand. Default values were considered for the van der Waals radii and the partial atomic charges.

Docking was performed using Glide in the Virtual Screening Wizard of the Schrodinger suite [44]. The specified default settings were considered for docking calculations. Ligands were docked using the OPLS 2005 force field and the option to output Glide XP descriptor information was chosen. Further, the option to write per-residue interaction scores for residues within 12 Å of receptor grid centre was also chosen. Finally, the protein–ligand complexes were subjected to post-docking minimization. The protein–ligand interactions, such as H-bonds and hydrophobic interactions, were visualized using LigPlot^{+} v.1.4 [45].

Feature evaluation (FE)

FE was carried out to check if all the energetically favourable pharmacophore features present in the CypD- binding site were extracted and also if the ligands interact with the amino acids corresponding to these features only [34]. This was achieved by analyzing the per-residue interactions of the top-best hits obtained through protein–ligand docking.

Per-residue interaction scores of amino acid residues were employed to calculate the H-bond energy contribution (HBEC) and total energy contribution (TEC) of amino acids within 12 Å of the receptor grid centre. HBEC denotes the H-bond energy contributed by each residue towards the interaction energy of ligands. Thus, all the amino acid residues that are involved in the H-bonding could be identified through HBEC. Similarly, TEC denotes the total interaction energy contributed by each amino acid residue with the ligands. This would help in identifying the residues that contributed more to the interaction energy of the ligands. The HBEC of an amino acid was calculated by adding the H-bond energies of all the ligands with that amino acid, and the TEC of an amino acid was calculated by adding the interaction energies of all the ligands with that amino acid.

$$\text{HBEC of an amino acid X} = \sum_{N=1}^{50} (\text{hydrogen bonding energy of ligand N with amino acid X}),$$

$$\text{TEC of an amino acid X} = \sum_{N=1}^{50} (\text{interaction energy of ligand N with amino acid X}),$$

where N is the number of ligands.

The HBEC and TEC of each amino acid were calculated for the top 50 ligands obtained through protein–ligand docking.

Protein–ligand–protein docking

To study the influence of CsA and other ligands on the CypD–p53 interactions, protein–ligand–protein docking was carried out by docking p53 with CypD–CsA or CypD–ligand complexes. Protein–ligand–protein docking was performed through the ZDOCK server as mentioned earlier in the protein–protein docking section. The docked complexes were further subjected to MD simulation studies.

MD simulation

Many marvellous biological functions in proteins and DNA and their profound dynamic mechanisms, such as switch between active and inactive states [46], cooperative effects [47], allosteric transition [48,49], intercalation of drugs into DNA [50] and assembly of microtubules [51], can be revealed by studying their internal motions, as elaborated in a comprehensive review and summarized in a recent paper [52,53] as well as a Wikipedia article at http://en.wikipedia.org/wiki/Low-frequency_collective_motion_in_proteins_and_DNA. Likewise, to really understand the action mechanism of receptor–ligand or protein–protein binding, we should consider not only the static structures concerned but also the dynamical information obtained by simulating their internal motions or dynamic process. To realize this, MD simulation is one of the feasible tools.

MD simulations of the protein–protein (CypD–p53), protein–ligand (CypD–ligand) and protein–ligand–protein (CypD–ligand–p53) complexes were carried out using the Gromacs v4.5.5 software with the Gromos53a6 force field [54–56]. The PRODRG server was used to generate the topologies and parameters for the ligands [57].

The system was initially subjected to 20,000 steps of steepest descent minimization in vacuum, followed by explicit solvation in a cubical water system. Simple point charge water molecules (SPC/E) were used for solvation and the protein complex was placed in the centre of a cubic box. The system was prepared by protonating the ionizable residues of the protein without artefacts. Neutralization of the system was achieved by the addition of Na^{+} and Cl^{-} counter ions and a salt concentration of 0.1 M NaCl. Linear constraint (LINCS) algorithm was applied to fix all the hydrogen-related bond lengths, facilitating the use of a 2-fs time step. Particle Mesh Ewald (PME) was employed to treat long-range electrostatic interactions [58]. A cut-off of 1.4 nm was used for both the Van der Waals and the PME component of electrostatic interactions. All the bond lengths associated with H-atoms were constrained through the SHAKE algorithm. Further, 20,000 steps of steepest descent energy minimization were employed on the solvated system.

After energy minimization, the system was equilibrated for 100 ps with NVT and NPT ensemble equilibration protocol for about 50,000 steps. Extensive MD simulations were then performed for about 20–60 ns under a constant number of particles at constant temperature and pressure, as previously described [34]. Analyses, such as RMSD and distances, were carried out using the tools bundled with the Gromacs distribution package and the visual molecular dynamics (VMD) analysis package [59].

Results and discussion

p53 protein structure

The complete protein sequence of p53 with 393 amino acids was retrieved from UniProt (ID: P04637) and its 3D structure was determined through threading. The predicted structure showed nearly 85 % of its residues in the most favoured regions of the Ramachandran plot (Online Resource 1). This p53 protein structure was docked with CypD to study the CypD–p53 interactions.

p53 binds to CypD at its CsA-binding site

CypD was docked with p53 and the resultant complex was subjected to 60 ns MD simulation. It was identified that p53 binds to CypD at its CsA-binding site (amino acid residues 60–80) (Fig. 2). This is in accordance with a previous study, which reported that p53 binds at the CsA-binding site of the cyclophilin protein, Cyp18 [60]. It can be deduced that this might be the reason behind the inhibition of CypD–p53 interaction by CsA. Thus, CsA may bind to CypD and block its binding site making it unavailable to p53.

The information of the binding site/binding pocket of a receptor for its ligand is very important for drug design, particularly for conducting mutagenesis studies [33]. In the literature, the binding pocket of a protein receptor to a ligand is usually defined by those residues that have at least one heavy atom (i.e., an atom other than hydrogen) within a distance of 5 Å from a heavy atom of the ligand. Such a criterion was originally used to define the binding pocket of ATP in the Cdk5–Nck5a* complex [61] that later proved quite useful in identifying functional domains and stimulating the relevant truncation experiments [62]. A similar approach has also been used to define the binding pockets of many other receptor–ligand interactions important for drug design [28,63–69].

Analysis of the CypD–p53 protein complex showed that these proteins are almost perfectly fitting to each other (Online Resource 2). p53 has a palm and thumb structure that accommodates CypD in the palm and fixes it using the thumb. In addition, the binding of p53 distorted the binding site of CypD (Fig. 2). The results of the MD simulation of the CypD–p53 complex showed that the RMSD of the protein complex as well as the individual proteins was steady and they became stable during the course of simulation (Fig. 3a–c). The RMSD of CypD, p53 and CypD–p53 complex was about 0.3, 0.8 and 1.5 nm, respectively. Further, the distance between these proteins decreased during the simulation, which supports the binding of CypD with p53 (Fig. 3d). Visual analysis of the simulation depicted that p53 came close and bound to CypD, as shown in the animation (Online Resource 3). However, the final distance is not zero and remains about 3.5 nm, since the distance was calculated between the centres of the two proteins (Fig. 3d).

CsA could inhibit the CypD–p53 interaction

It was reported that CsA inhibited the CypD–p53 interactions and, in this study, we have observed that p53 binds to CypD at the CsA- binding site. By combining these two events, we attempted to deduce the mechanism behind the inhibition of CypD–p53 interaction by CsA. We propose that binding of CsA might block the binding site of CyPD from p53. Further, we wondered whether this logic could be replicated through MD simulation studies. Hence, p53 was docked to the CypD–CsA complex (PDB Id: 2Z6W) and the resulting CypD–CsA–p53 complex was subjected to 40 ns MD simulation.

As expected, CsA could inhibit the CypD–p53 interaction. It was observed that, in the presence of CsA, CypD could not bind to p53. This supports our proposal that p53 binds to CypD at its binding site. Hence, this interaction could be inhibited by CsA since it blocks the CypD-binding site and makes it unavailable for the binding of p53.

The RMSD of CypD and p53 was 0.3 and 0.8 nm, respectively (Fig. 4a, b). Though they were similar to their respective RMSD observed during CypD–p53 simulation (Fig. 3a, b), the RMSD of p53 was not at all stable and it increased as the simulation progressed. In addition, compared to CypD, p53 was not stable and its structure varied a lot. The RMSD of the protein complex was approximately 4 nm and it was also not at all stable and varied greatly throughout the simulation (Fig. 4d). This shows that a stable CypD–p53 complex was not formed during the simulation. Further, during the course of simulation, the distance between CypD and p53 increased and both the proteins were separated by 7 nm (Fig. 4e). This shows that, in the presence of CsA, p53 could not bind to CypD and both the proteins move away from each other, as shown in the animation (Online Resource 4).

The RMSD of CsA was 0.2 nm and it became stable during the simulation (Fig. 4c). The distance between CypD and CsA was 1.2 nm. It did not vary much and became stable during simulation (Fig. 4f). This demonstrates that CypD was

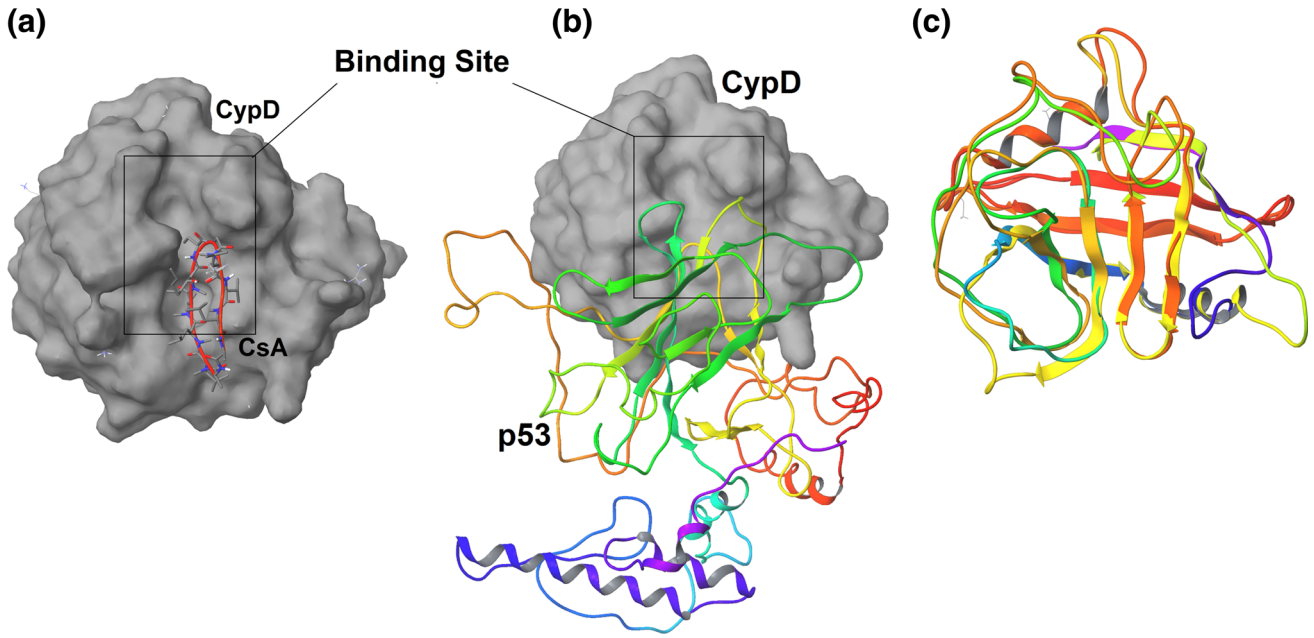

Fig. 2 Comparison of the CypD-binding site structure **a** CypD bound to CsA, **b** CypD bound to p53 and **c** structural alignment of CypD structures bound and unbound to p53

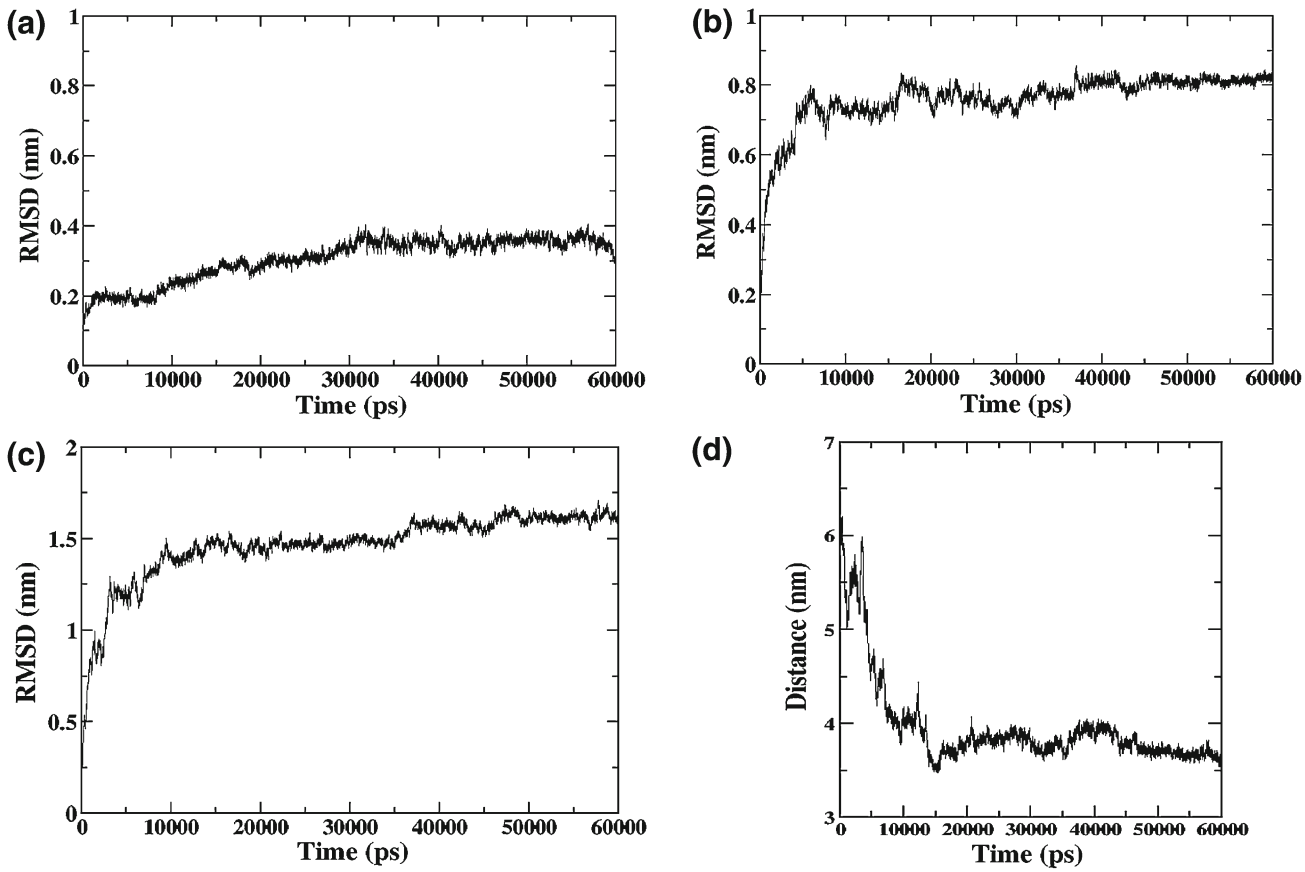

Fig. 3 MD simulation results of CypD–p53 complex **a** RMSD of CypD, **b** RMSD of p53, **c** RMSD of CypD–p53 complex and **d** distance between CypD and p53

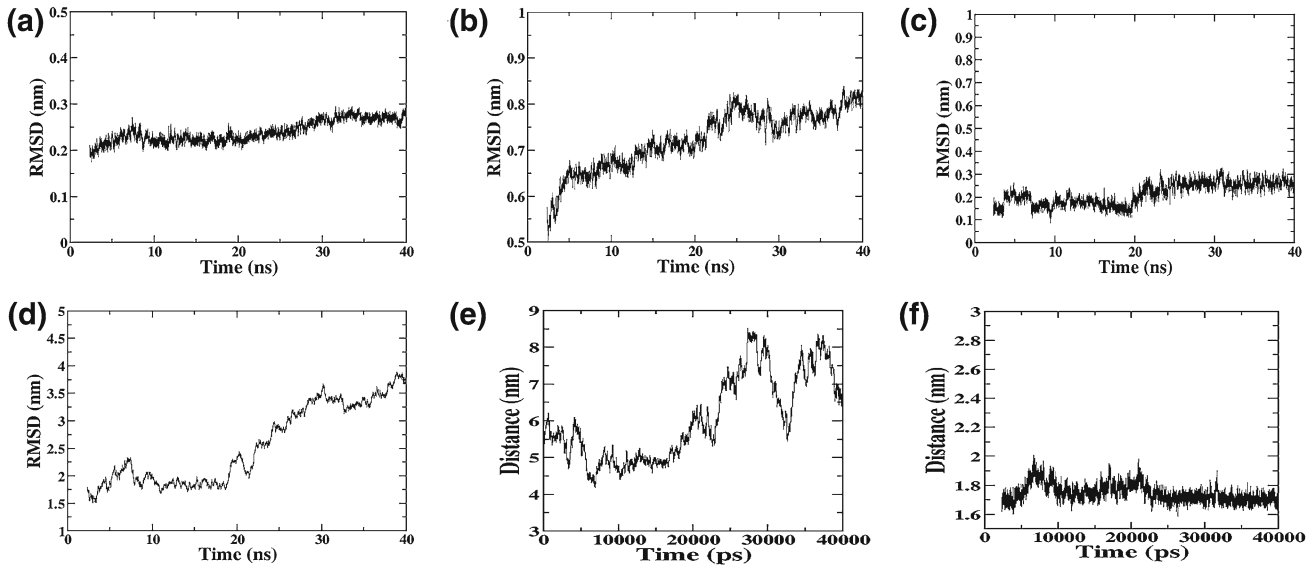

Fig. 4 MD simulation results of CypD–CsA–p53 complex **a** RMSD of CypD, **b** RMSD of p53, **c** RMSD of CsA, **d** RMSD of CypD–p53 complex, **e** distance between CypD and p53 and **f** distance between CypD and CsA

close to CsA than p53. Further, The final position of CsA was almost similar to its initial position, which indicates that CsA remains in the binding site of CypD (Fig. 4f). Taken together, it could be inferred that CsA binds to CypD and forms a stable complex, which in turn inhibits p53 from binding to CypD. Visual analysis of the simulation depicted that CsA binds to CypD and remains in the binding site throughout the simulation. Moreover, p53 does not bind to CypD and moves away from it (Online Resource 4).

Therefore, this logic/mechanism that the presence of a molecule/inhibitor at the CsA-binding site of CypD may inhibit the CypD–p53 interactions could be employed to identify small molecule CypD inhibitors that may inhibit these protein–protein interactions.

CypD e-pharmacophore

Structure-based drug design approach was adopted to identify the CypD inhibitors. Fragment-based e-pharmacophore was extracted from the CypD-binding site to identify all the energetically favourable pharmacophoric features. The extracted pharmacophore contained ten features, AAAADDDDRR (Fig. 5). These features were corresponding to the amino acids Arg 55, Gln 63, Gly 72, Asn 102, Ser 110, Gln 111 and His 126 (Fig. 5a, b) (Online Resource 5). Most of these amino acids are involved in the interaction of CypD with CsA.

This pharmacophore was validated using the EF. The $EF^{1\%}$ and $EF^{5\%}$ were 20 and 6, respectively. This shows that the extracted pharmacophore is considerably reliable. Finally, pharmacophore-based screening of ZINC database retrieved approximately 0.3 million compounds.

Docking-based virtual screening

The compound hits obtained through pharmacophore-based screening were further screened through high throughput virtual screening (HTVS), standard precision (SP) and extra precision (XP) docking. Ligands were chosen for MD simulation based on their glide score and glide energy. Ligand 1 or Ligand S is the top-best and the strongest binding ligand that showed good glide score and glide energy (Table 1). The top ligands aligned well with most of the features in the e-pharmacophore (Online Resource 6) and also showed interactions with the amino acids corresponding to the pharmacophoric features (Fig. 6). The alignment of CypD–Ligand1 complexes, obtained through docking and simulation, shows that the ligand binds to the protein with similar conformational modes (Online Resource 7) and this confirms the interactions of the ligands obtained during docking studies.

Feature evaluation

FE was carried out to identify the amino acids that are involved in H-bonding with the ligands and that contributes more to the binding of the ligand with the protein. HBEC graph (Online Resource 8) of the top-most 50 ligands shows that the amino acid residues 55, 63, 72, 74, 101, 102 and 111 are involved in H-bonding. Amino acids 102 and 101 form H-bonds with the maximum and minimum number of ligands, respectively (Online Resource 8). Almost all these residues are the amino acids corresponding to the pharmacophoric features.

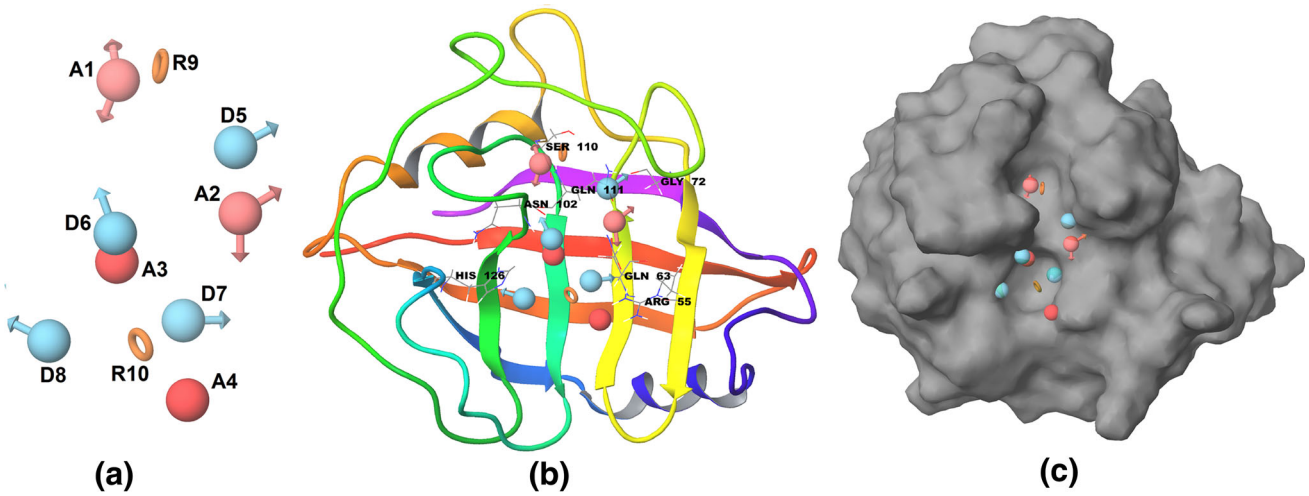

Fig. 5 CypD e-pharmacophore **a** AAAADDDDRR pharmacophoric features, **b** pharmacophoric features and their corresponding/interacting amino acids and **c** pharmacophoric features mapped onto the CypD-binding site

Table 1 Docking results of the top three ligand molecules

Ligand	Zinc ID	Glide score	Glide energy (Kcal/mol)	H-bond interactions
Ligand 1	ZINC76567082	−8.581706	−51.789667	Gln 63, Asn 102, Gly 109, Ser 110, Gln 111
Ligand 2	ZINC79129464	−8.159309	−51.796525	Gln 63, Gly 72, Ser 110, Gln 111
Ligand 3	ZINC51336509	−8.141029	−50.572725	Gln 63, Ala 101, Asn 102

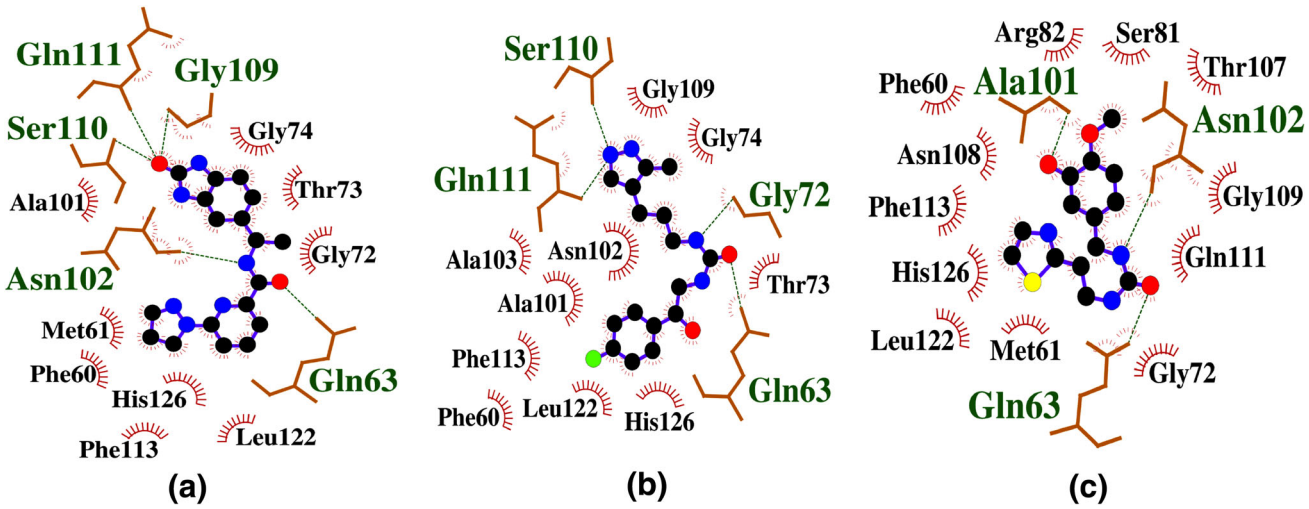

Fig. 6 H-bonds and hydrophobic interactions of the top three ligands with the amino acids present in the binding site **a** Ligand 1 (Ligand S), **b** Ligand 2 and **c** Ligand 3

TEC was calculated for the seven amino acids that are involved in H-bonding. TEC graph illustrates that Asn 102 contributed to a greater extent for the total binding energy of the top-most ligands (Online Resource 9). Thus, the HBEC and TEC analysis demonstrates that almost all the pharmacophoric features required for the binding of ligands were extracted from the CypD-binding site.

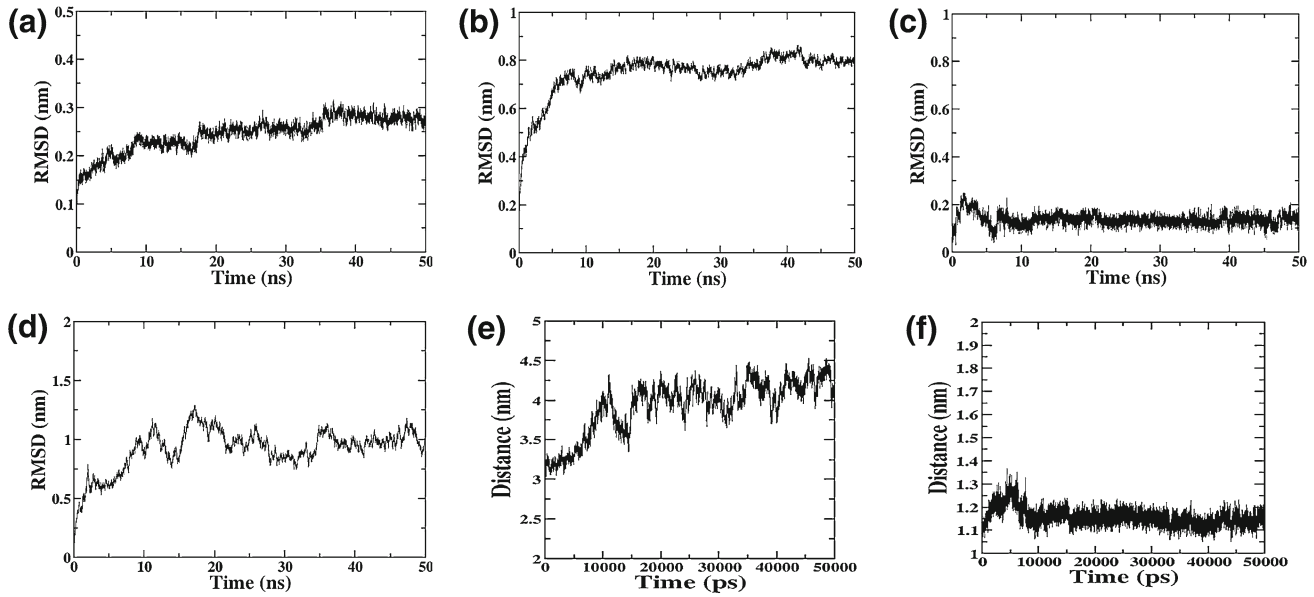

Fig. 7 MD simulation results of CypD–Ligand1–p53 complex **a** RMSD of CypD, **b** RMSD of p53, **c** RMSD of Ligand 1, **d** RMSD of CypD–p53 complex, **e** distance between CypD and p53 and **f** distance between CypD and Ligand 1

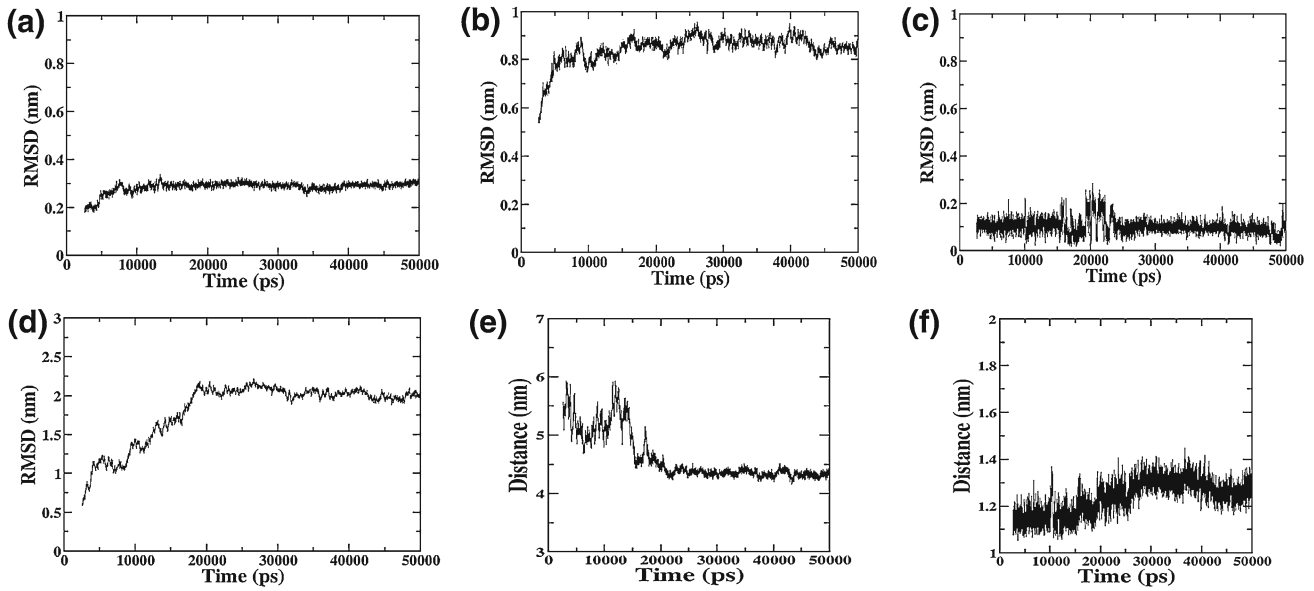

Fig. 8 MD simulation results of CypD–LigandW–p53 complex **a** RMSD of CypD, **b** RMSD of p53, **c** RMSD of Ligand W, **d** RMSD of CypD–p53 complex, **e** distance between CypD and p53 and **f** distance between CypD and Ligand W

Strong ligand of CypD inhibited CypD–p53 interactions

We employed a similar strategy, as in the case of CsA, to test whether the top-most ligand obtained through docking could inhibit the CypD–p53 interactions. CypD–Ligand1 complex was docked with p53 and the resulting CypD–Ligand1–p53 complex was subjected to 50 ns MD simulation.

The RMSD of p53 was not stable during the simulation (Fig. 7b). In addition, the RMSD of the protein complex was also not at all stable and varied a lot throughout the simulation (Fig. 7d). This illustrates that a stable CypD–p53 complex was not formed during the simulation. Further, the distance between CypD and p53 increased up to 4.5 nm during the course of simulation, indicating that p53 does not bind to CypD (Fig. 7e). Thus, in the presence of Ligand 1, both the proteins do not bind and also move away from each other, as shown in the animation (Online Resource 10).

Comparison of distances between CypD and p53 during CypD–CsA–p53 and CypD–Ligand1–p53 simulations (Figs. 4e, 7e) demonstrates that these two proteins were separated to a greater extent by CsA when compared to Ligand 1. This might be due to CsA is a large bulky peptide molecule, whereas Ligand 1 is a small molecule. However, it should be noted that both CsA and Ligand 1 were able to inhibit the CypD–p53 interactions.

The RMSD of Ligand 1 was 0.2 nm and it became stable during the simulation (Fig. 7c). The distance between CypD and Ligand 1 was 1.2 nm, which demonstrates that CypD was close to CsA than p53 (Fig. 7f). It could be observed that the distances of CypD–CsA and CypD–Ligand1 are similar (Figs. 4f, 7f). Further, the distance between CypD and Ligand 1 did not vary much and the final position of the ligand was almost similar to its initial position (Fig. 7f), which shows that Ligand 1 remained bound within the CypD-binding site. The RMSD and distance profiles of CypD–Ligand1–p53 simulation were similar to those in the case of CypD–CsA–p53 simulation. Visual analysis of the simulation depicted that Ligand 1 binds to CypD and remains in the binding site throughout the simulation. However, p53 does not bind to CypD and moves away from it (Online Resource 10). Therefore, it could be deduced that Ligand 1 binds to CypD and inhibits its interaction with p53, in a way similar to CsA.

Weak ligand of CypD could not inhibit CypD–p53 interactions

We wondered how CypD and p53 would act in the presence of a weak ligand (Ligand W). Is it really the interaction of Ligand 1 with CypD or is it merely because of the presence of a ligand at the CypD–p53 interface that inhibited the CypD–p53 interaction? To answer this question, MD simulation was carried out on CypD–LigandW–p53 complex.

Ligand W was not able to inhibit the CypD–p53 interactions. The RMSD of the CypD–p53 protein complex as well as the individual proteins was steady and they became stable during the course of simulation (Fig. 8). The RMSD of CypD, p53 and CypD–p53 complex were about 0.3 nm, 0.8 nm and 2.0 nm, respectively. Though the RMSD of the Ligand W was 0.2 nm, it varied a lot throughout the simulation.

The distance between CypD and p53 decreased and became stable during the simulation, which supports the binding of CypD with p53 (Fig. 8e). Conversely, the distance between CypD and Ligand W increased up to 1.4 nm and was not stable. Here, it could be observed that the distance between CypD–LigandW is less than the distance between CypD–p53. This gives an impression that the Ligand W remains close to CypD and binds to it. Nevertheless, visual analysis of the simulation showed that Ligand W did not bind

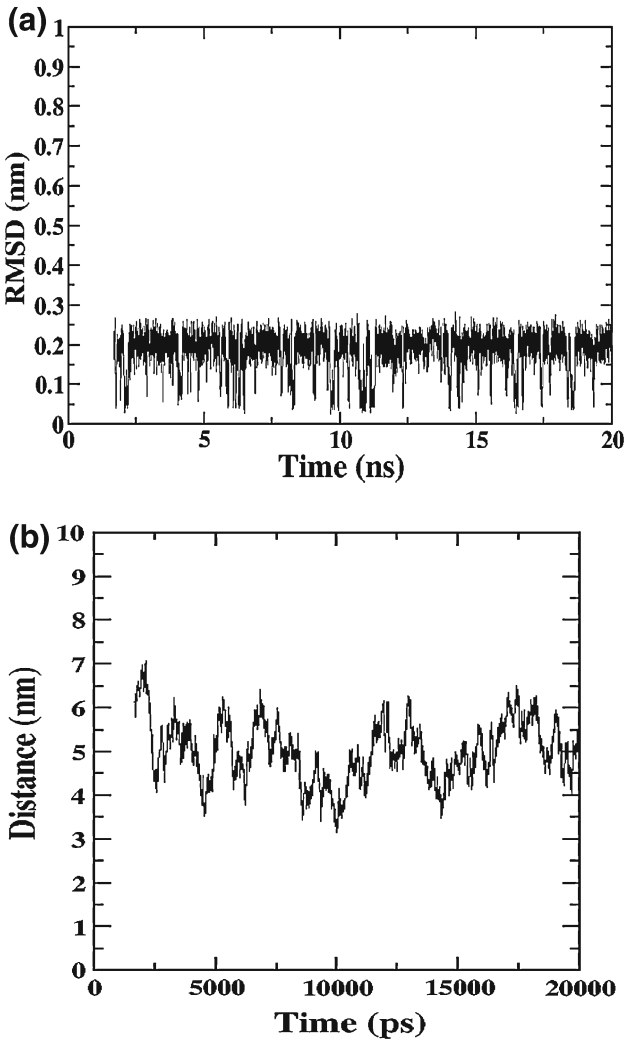

Fig. 9 MD simulation results of CypD–LigandW complex **a** RMSD of Ligand W and **b** distance between CypD and Ligand W

to CypD properly and it tried to move out of the binding site, as shown in the animation (Online Resource 11). However, it was struck between the CypD and p53 proteins and so could not move away from CypD.

In order to unravel whether Ligand W really binds to CypD or is it because of p53 that it remained close to CypD, we performed MD simulation of CypD–LigandW complex for 20 ns. It was observed that Ligand W does not bind to CypD and it moved away from the binding site, as shown in the animation (Online Resource 12). The RMSD of Ligand W was not at all stable and varied throughout the simulation (Fig. 9a). Further, the distance between CypD and Ligand W was approximately 6.5 nm, which is very high (Fig. 9b).

Thus, the RMSD and distance profiles of CypD–LigandW–p53 simulation were similar to those in the case of CypD–p53 simulation. Hence, it could be deduced that, in the presence of Ligand W, CypD–p53 complex is formed and Ligand W could not inhibit this interaction.

Conclusions

Protein–protein interactions (PPI) are central in the cause and progress of a variety of diseases. Knowledge regarding the underlying molecular mechanisms is necessary to understand and inhibit these interactions. CypD–p53 interaction is crucial for MPTP formation and necroptosis. The information that this interaction could be inhibited by CsA, ignited the idea that CypD inhibitors could regulate necroptosis pathway. Given the limitations of CsA, there is a need to discover novel small molecular CypD inhibitors. However, no information is available regarding the CypD–p53 interactions and their binding modes. Further, the mechanism of action of CsA is not known.

In this study, we have modelled the molecular mechanism of CypD–p53 inhibition by CsA. It was identified that p53 binds to CypD at its CsA-binding site and thus CsA could inhibit this interaction. In addition, e-pharmacophore was extracted from the CypD-binding site and was employed to screen compounds. Potential inhibitors were identified through docking and MD simulation studies. The top-most ligand (Ligand 1) was validated through similar strategy, which was used during the modelling of CsA activity. Further, this modelling methodology was checked through a weak ligand. It was identified that the strong ligand was able to inhibit the CypD–p53 interaction, in a way much similar to CsA. Conversely, the weak ligand was not able to inhibit this interaction. In the presence of the weak ligand, p53 came close to CypD and they interacted similarly to their native interaction, suggesting that the weak ligand has no influence. Thus, through this study, we have proposed a computational strategy that could be employed to study and delineate the molecular mechanism of protein–protein interactions and their inhibition. Further, this strategy could be employed in the identification and evaluation of novel inhibitors of PPI.

Compliance with Ethical Standards

Conflicts of interest The authors declare that they have no conflict of interest.

Funding This study was funded by the Department of Biotechnology, Government of India "Bioinformatics Infrastructure Facility for Biology Teaching through Bioinformatics (BIF-BTBI)" (Grant number: BT/BI/25/001/2006 dated 25/03/2011).

References

1. Vaseva AV, Marchenko ND, Ji K, Tsirka SE, Holzmann S, Moll UM (2012) p53 opens the mitochondrial permeability transition pore to trigger necrosis. Cell 149:1536–1548. doi:10.1016/j.cell.2012.05.014
2. Baines CP, Kaiser RA, Purcell NH, Blair NS, Osinska H, Hambleton MA, Brunskill EW, Sayen MR, Gottlieb RA, Dorn GW, Robbins J, Molkentin JD (2005) Loss of cyclophilin D reveals a critical role for mitochondrial permeability transition in cell death. Nature 434:658–662. doi:10.1038/nature03434
3. Basso E, Fante L, Fowlkes J, Petronilli V, Forte MA, Bernardi P (2005) Properties of the permeability transition pore in mitochondria devoid of cyclophilin D. J Biol Chem 280:18558–18561. doi:10.1074/jbc.C500089200
4. Kumarswamy R, Chandna S (2009) Putative partners in Bax mediated cytochrome-c release: ANT, CypD, VDAC or none of them? Mitochondrion 9:1–8. doi:10.1016/j.mito.2008.10.003
5. Du H, Yan SS (2010) Mitochondrial permeability transition pore in Alzheimer's disease: cyclophilin D and amyloid beta. Biochim Biophys Acta 1802:198–204. doi:10.1016/j.bbadis.2009.07.005
6. Baines CP (2007) The mitochondrial permeability transition pore as a target of cardioprotective signaling. Am J Physiol Heart Circ Physiol 293:H903–H904. doi:10.1152/ajpheart.00575.2007
7. Du H, Guo L, Fang F, Chen D, Sosunov AA, McKhann GM, Yan Y, Wang C, Zhang H, Molkentin JD, Gunn-Moore FJ, Vonsattel JP, Arancio O, Chen JX, Yan SD (2008) Cyclophilin D deficiency attenuates mitochondrial and neuronal perturbation and ameliorates learning and memory in Alzheimer's disease. Nat Med 14:1097–1105. doi:10.1038/nm.1868
8. Martin LJ, Semenkow S, Hanaford A, Wong M (2014) The mitochondrial permeability transition pore regulates Parkinson's disease development in mutant α-synuclein transgenic mice. Neurobiol Aging 35:1132–1152. doi:10.1016/j.neurobiolaging.2013.11.008
9. Shirendeb U, Reddy AP, Manczak M, Calkins MJ, Mao P, Tagle DA, Reddy PH (2011) Abnormal mitochondrial dynamics, mitochondrial loss and mutant huntingtin oligomers in Huntington's disease: implications for selective neuronal damage. Hum Mol Genet 20:1438–1455. doi:10.1093/hmg/ddr024
10. Schinzel AC, Takeuchi O, Huang Z, Fisher JK, Zhou Z, Rubens J, Hetz C, Danial NN, Moskowitz MA, Korsmeyer SJ (2005) Cyclophilin D is a component of mitochondrial permeability transition and mediates neuronal cell death after focal cerebral ischemia. Proc Natl Acad Sci USA 102:12005–12010. doi:10.1073/pnas.0505294102
11. Sullivan PG, Rabchevsky AG, Waldmeier PC, Springer JE (2005) Mitochondrial permeability transition in CNS trauma: cause or effect of neuronal cell death? J Neurosci Res 79:231–239. doi:10.1002/jnr.20292
12. Nakagawa T, Shimizu S, Watanabe T, Yamaguchi O, Otsu K, Yamagata H, Inohara H, Kubo T, Tsujimoto Y (2005) Cyclophilin D-dependent mitochondrial permeability transition regulates some necrotic but not apoptotic cell death. Nature 434:652–658. doi:10.1038/nature03317
13. Martin LJ (2011) An approach to experimental synaptic pathology using green fluorescent protein-transgenic mice and gene knockout mice to show mitochondrial permeability transition pore-driven excitotoxicity in interneurons and motoneurons. Toxicol Pathol 39:220–233. doi:10.1177/0192623310389475
14. Uchino H, Elmér E, Uchino K, Li PA, He QP, Smith ML, Siesjö BK (1998) Amelioration by cyclosporin A of brain damage in transient forebrain ischemia in the rat. Brain Res 812:216–226. doi:10.1016/S0006-8993(98)00902-0
15. Matsuda S, Moriguchi T, Koyasu S, Nishida E (1998) T lymphocyte activation signals for interleukin-2 production involve activation of MKK6-p38 and MKK7-SAPK/JNK signaling pathways sensitive to cyclosporin A. J Biol Chem 273:12378–12382. doi:10.1074/jbc.273.20.12378
16. Liu J, Farmer JD Jr, Lane WS, Friedman J, Weissman I, Schreiber SL (1991) Calcineurin is a common target of cyclophilin-cyclosporin A and FKBP-FK506 complexes. Cell 66:807–815. doi:10.1016/0092-8674(91)90124-H
17. Lee SP, Hwang YS, Kim YJ, Kwon KS, Kim HJ, Kim K, Chae HZ (2001) Cyclophilin a binds to peroxiredoxins and activates its

peroxidase activity. J Biol Chem 276:29826–29832. doi:10.1074/jbc.M101822200
18. Matsuda S, Shibasaki F, Takehana K, Mori H, Nishida E, Koyasu S (2000) Two distinct action mechanisms of immunophilin-ligand complexes for the blockade of T-cell activation. EMBO Rep 1:428–434. doi:10.1093/embo-reports/kvd090
19. Margulies S, Hicks R, Combination Therapies for Traumatic Brain Injury Workshop Leaders (2009) Combination therapies for traumatic brain injury: prospective considerations. J Neurotrauma 26:925–939. doi:10.1089/neu.2008-0794
20. Roy A, Kucukural A, Zhang Y (2010) I-TASSER: a unified platform for automated protein structure and function prediction. Nat Protoc 5:725–738. doi:10.1038/nprot.2010.5
21. Schnell JR, Chou JJ (2008) Structure and mechanism of the M2 proton channel of influenza A virus. Nature 451:591–595. doi:10.1038/nature06531
22. Berardi MJ, Shih WM, Harrison SC, Chou JJ (2011) Mitochondrial uncoupling protein 2 structure determined by NMR molecular fragment searching. Nature 476:109–113. doi:10.1038/nature10257
23. OuYang B, Xie S, Berardi MJ, Zhao X, Dev J, Yu W, Sun B, Chou JJ (2013) Unusual architecture of the p7 channel from hepatitis C virus. Nature 498:521–525. doi:10.1038/nature12283
24. Call ME, Schnell JR, Xu C, Lutz RA, Chou JJ, Wucherpfennig KW (2006) The structure of the zetazeta transmembrane dimer reveals features essential for its assembly with the T cell receptor. Cell 127:355–368. doi:10.1016/j.cell.2006.08.044
25. Wang J, Pielak RM, McClintock MA, Chou JJ (2009) Solution structure and functional analysis of the influenza B proton channel. Nat Struct Mol Biol 16:1267–1271. doi:10.1038/nsmb.1707
26. Call ME, Wucherpfennig KW, Chou JJ (2010) The structural basis for intramembrane assembly of an activating immunoreceptor complex. Nat Immunol 11:1023–1029. doi:10.1038/ni.1943
27. Chou KC, Jones D, Heinrikson RL (1997) Prediction of the tertiary structure and substrate binding site of caspase-8. FEBS Lett 419:49–54. doi:10.1016/S0014-5793(97)01246-5
28. Wang SQ, Du QS, Chou KC (2007) Study of drug resistance of chicken influenza A virus (H5N1) from homology-modeled 3D structures of neuraminidases. Biochem Biophys Res Commun 354:634–640. doi:10.1016/j.bbrc.2006.12.235
29. Chou KC, Tomasselli AG, Heinrikson RL (2000) Prediction of the tertiary structure of a caspase-9/inhibitor complex. FEBS Lett 470:249–256. doi:10.1016/S0014-5793(00)01333-8
30. Wang JF, Wei DQ, Li L, Zheng SY, Li YX, Chou KC (2007) 3D structure modeling of cytochrome P450 2C19 and its implication for personalized drug design. Biochem Biophys Res Commun 355:513–519. doi:10.1016/j.bbrc.2007.01.185
31. Chou KC (2005) Coupling interaction between thromboxane A2 receptor and alpha-13 subunit of guanine nucleotide-binding protein. J Proteome Res 4:1681–1686. doi:10.1021/pr050145a
32. Wang SQ, Du QS, Huang RB, Zhang DW, Chou KC (2009) Insights from investigating the interaction of oseltamivir (Tamiflu) with neuraminidase of the 2009 H1N1 swine flu virus. Biochem Biophys Res Commun 386:432–436. doi:10.1016/j.bbrc.2009.06.016
33. Chou KC (2004) Structural bioinformatics and its impact to biomedical science. Curr Med Chem 11:2105–2134. doi:10.2174/0929867043364667
34. Fayaz SM, Rajanikant GK (2014) Ensemble pharmacophore meets ensemble docking: a novel screening strategy for the identification of RIPK1 inhibitors. J Comput Aided Mol Des 28:779–794. doi:10.1007/s10822-014-9771-x
35. Chou KC, Cai YD (2006) Predicting protein-protein interactions from sequences in a hybridization space. J Proteome Res 5:316–322. doi:10.1021/pr050331g
36. Hu L, Huang T, Shi X, Lu WC, Cai YD, Chou KC (2011) Predicting functions of proteins in mouse based on weighted protein-protein interaction network and protein hybrid properties. PLoS One 6:e14556. doi:10.1371/journal.pone.0014556
37. Huang T, Chen L, Cai YD, Chou KC (2011) Classification and analysis of regulatory pathways using graph property, biochemical and physicochemical property, and functional property. PLoS One 6:e25297. doi:10.1371/journal.pone.0025297
38. Li BQ, Huang T, Liu L, Cai YD, Chou KC (2012) Identification of colorectal cancer related genes with mRMR and shortest path in protein-protein interaction network. PLoS One 7:e33393. doi:10.1371/journal.pone.0033393
39. Jia J, Liu Z, Xiao X, Liu B, Chou KC (2015) iPPI-Esml: an ensemble classifier for identifying the interactions of proteins by incorporating their physicochemical properties and wavelet transforms into PseAAC. J Theor Biol 377:47–56. doi:10.1016/j.jtbi.2015.04.011
40. Pierce BG, Wiehe K, Hwang H, Kim BH, Vreven T, Weng Z (2014) ZDOCK server: interactive docking prediction of protein-protein complexes and symmetric multimers. Bioinformatics 30:1771–1773. doi:10.1093/bioinformatics/btu097
41. Bender A, Glen RC (2005) A discussion of measures of enrichment in virtual screening: comparing the information content of descriptors with increasing levels of sophistication. J Chem Inf Model 45:1369–1375. doi:10.1021/ci0500177
42. Jain AN, Nicholls A (2008) Recommendations for evaluation of computational methods. J Comput Aided Mol Des 22:133–139. doi:10.1007/s10822-008-9196-5
43. Irwin JJ, Shoichet BK (2005) ZINC—a free database of commercially available compounds for virtual screening. J Chem Inf Model 45:177–182. doi:10.1021/ci049714
44. Friesner RA, Banks JL, Murphy RB, Halgren TA, Klicic JJ, Mainz DT, Repasky MP, Knoll EH, Shelley M, Perry JK, Shaw DE, Francis P, Shenkin PS (2004) Glide: a new approach for rapid, accurate docking and scoring. 1. Method and assessment of docking accuracy. J Med Chem 47:1739–1749. doi:10.1021/jm0306430
45. Laskowski RA, Swindells MB (2011) LigPlot^{+}: multiple ligand-protein interaction diagrams for drug discovery. J Chem Inf Model 51:2778–2786. doi:10.1021/ci200227u
46. Wang JF, Chou KC (2009) Insight into the molecular switch mechanism of human Rab5a from molecular dynamics simulations. Biochem Biophys Res Commun 390:608–612. doi:10.1016/j.bbrc.2009.10.014
47. Chou KC (1989) Low-frequency resonance and cooperativity of hemoglobin. Trends Biochem Sci 14:212–213. doi:10.1016/0968-0004(89)90026-1
48. Wang JF, Gong K, Wei DQ, Li YX, Chou KC (2009) Molecular dynamics studies on the interactions of PTP1B with inhibitors: from the first phosphate-binding site to the second one. Protein Eng Des Sel 22:349–355. doi:10.1093/protein/gzp012
49. Chou KC (1987) The biological functions of low-frequency phonons: 6. A possible dynamic mechanism of allosteric transition in antibody molecules. Biopolymers 26:285–295. doi:10.1002/bip.360260209
50. Chou KC, Mao B (1988) Collective motion in DNA and its role in drug intercalation. Biopolymers 27:1795–1815. doi:10.1002/bip.360271109
51. Chou KC, Zhang CT, Maggiora GM (1994) Solitary wave dynamics as a mechanism for explaining the internal motion during microtubule growth. Biopolymers 34:143–153. doi:10.1002/bip.360340114
52. Chou KC (1988) Low-frequency collective motion in biomacromolecules and its biological functions. Biophys Chem 30:3–48. doi:10.1016/0301-4622(88)85002-6
53. Lin SX, Lapointe J (2013) Theoretical and experimental biology in one. J Biomed Sci Eng 6:435–442. doi:10.4236/jbise.2013.64054
54. Van Der Spoel D, Lindahl E, Hess B, Groenhof G, Mark AE, Berendsen HJ (2005) GROMACS: fast, flexible, and free. J Comput Chem 26:1701–1718. doi:10.1002/jcc.20291
55. Hess B, Kutzner C, van der Spoel D, Lindahl E (2008) GROMACS 4: algorithms for highly efficient, load-balanced, and scalable mole-

cular simulation. J Chem Theory Comput 4:435–447. doi:10.1021/ct700301q
56. Oostenbrink C, Villa A, Mark AE, van Gunsteren WF (2004) A biomolecular force field based on the free enthalpy of hydration and solvation: the GROMOS force-field parameter sets 53A5 and 53A6. J Comput Chem 25:1656–1676. doi:10.1002/jcc.20090
57. van Aalten DM, Bywater R, Findlay JB, Hendlich M, Hooft RW, Vriend G (1996) PRODRG, a program for generating molecular topologies and unique molecular descriptors from coordinates of small molecules. J Comput Aided Mol Des 10:255–262. doi:10.1007/BF00355047
58. Darden T, York D, Pedersen L (1993) Particle mesh Ewald—an N. log(N) method for ewald sums in large systems. J Chem Phys 98:10089–10093. doi:10.1063/1.464397
59. Humphrey W, Dalke A, Schulten K (1996) VMD: visual molecular dynamics. J Mol Graph 14:33–38. doi:10.1016/0263-7855(96)00018-5
60. Baum N, Schiene-Fischer C, Frost M, Schumann M, Sabapathy K, Ohlenschläger O, Grosse F, Schlott B (2009) The prolyl cis/trans isomerase cyclophilin 18 interacts with the tumor suppressor p53 and modifies its functions in cell cycle regulation and apoptosis. Oncogene 28:3915–3925. doi:10.1038/onc.2009.248
61. Chou KC, Watenpaugh KD, Heinrikson RL (1999) A model of the complex between cyclin-dependent kinase 5 (Cdk5) and the activation domain of neuronal Cdk5 activator. Biochem Biophys Res Commun 259:420–428. doi:10.1006/bbrc.1999.0792
62. Zhang J, Luan CH, Chou KC, Johnson GV (2002) Identification of the N-terminal functional domains of Cdk5 by molecular truncation and computer modeling. Proteins 48:447–453. doi:10.1002/prot.10173
63. Chou KC, Wei DQ, Zhong WZ (2003) Binding mechanism of coronavirus main proteinase with ligands and its implication to drug design against SARS. Biochem Biophys Res Commun 308:148–151. doi:10.1016/S0006-291X(03)01342-1
64. Huang RB, Du QS, Wang CH, Chou KC (2008) An in-depth analysis of the biological functional studies based on the NMR M2 channel structure of influenza A virus. Biochem Biophys Res Commun 377:1243–1247. doi:10.1016/j.bbrc.2008.10.148
65. Chou KC (2004) Molecular therapeutic target for type-2 diabetes. J Proteome Res 3:1284–1288. doi:10.1021/pr049849v
66. Li XB, Wang SQ, Xu WR, Wang RL, Chou KC (2011) Novel inhibitor design for hemagglutinin against H1N1 influenza virus by core hopping method. PLoS One 6:e28111. doi:10.1371/journal.pone.0028111
67. Wang JF, Chou KC (2011) Insights from modeling the 3D structure of New Delhi metallo-beta-lactamase and its binding interactions with antibiotic drugs. PLoS One 6:e18414. doi:10.1371/journal.pone.0018414
68. Wang JF, Chou KC (2012) Insights into the mutation-induced HHH syndrome from modeling human mitochondrial ornithine transporter-1. PLoS One 7:e31048. doi:10.1371/journal.pone.0031048
69. Pielak RM, Schnell JR, Chou JJ (2009) Mechanism of drug inhibition and drug resistance of influenza A M2 channel. Proc Natl Acad Sci USA 106:7379–7384. doi:10.1073/pnas.0902548106